

APPLICATION OF MICROANALYTICAL TECHNIQUES TO THE STUDY OF PRIMARY AND SECONDARY MINERALS IN TERRESTRIAL AND EXTRA-TERRESTRIAL ROCKS

EMILY JESSICA BATHGATE

A thesis in partial fulfilment of the requirements for the degree of

Master of Science (Research)

University of Technology Sydney

April 2019

I. Abstract

Many gaps in the understanding of the Martian regolith still exist. A full understanding of the history of the Martian climate and geology is important for our understanding of the history of the solar system and the evolution of planetary bodies and atmospheres. Two future missions to Mars will send Raman spectrometers to the surface of Mars in a search for biosignatures, signs of life and important minerals which indicate long term liquid water on the surface of the planet.

A Raman library has been compiled to complement and add to existing libraries; this library has subsequently been tested against Mars analogue materials: Icelandic tephra and three Australian meteorites. The minerals of these samples were also analysed to understand their original magmatic composition and potential metamorphism using Raman spectroscopy and other established techniques. This library further illustrated the difficulty of obtaining some mineral spectra (clays) that are important to the search for hydrated minerals. Testing of the library reinforced the strength of Raman spectroscopy in identifying constituent minerals of rocks and further inferring their chemistry and metamorphic history. The results of this study further illustrated the need for a dual nature to any *in-situ* research using Raman spectroscopy. The Raman spectrometer was able to detect some minerals that other techniques did not isolate, but the known fluorescence issues created problems when analysing some important minerals. Therefore, it is essential to pair Raman spectroscopy with other techniques such as infrared spectroscopy.

Analysis of our meteorite samples indicated that two of the samples originated from a different melt to the other and inferred a different temperature of formation. This knowledge is essential to the understanding of the formation history of the meteorite parent body. We can now constrain the temperature of formation of these meteorites and further work will focus on ascertaining the age of these meteorites through study of the baddeleyite grains found in the Binda meteorite.

II. List of Publications

Bathgate, E., Caprarelli, G., Xiao, L., Shimmmon, R., & Pogson, R. (2014) Raman characterisation of the products of alteration and low-grade metamorphism of volcanic rock minerals: preliminary results and implications for Martian studies. *Proceedings from 13th Australian Space Science Conference*, 2013, 97-108.

Bathgate, E., Maynard-Casely, H., Caprarelli, G., Xiao, L., Stuart, B., & Smith, K. (2014) Raman and XRD Study of Icelandic Tephra: Characterisation of Alteration Minerals and Implications for Mars, *11th International GeoRaman Conference. LPI Contributions*, St. Louis, Missouri., p. 5039.

Bathgate, EJ., Maynard-Casely, HE., Caprarelli, G., Xiao, L., Stuart, B., Smith, KT. & Pogson, R. (2015) Raman, FTIR and XRD study of Icelandic tephra minerals: implications for Mars, *Journal of Raman Spectroscopy*, vol. 46, no. 10, pp. 846-55. doi: 10.1002/jrs.4694.

Bathgate, EJ., Caprarelli, G., Xiao, L., Stuart, B., & Pogson, R. (2016) Raman, EPMA and SEM analysis of Meteorites from the Australian Museum, (Abstract) *16th Australian Space Research Conference Proceedings*, RMIT, Melbourne 2016.

III. Table of Contents

I.	ABSTRACT	I
II.	LIST OF PUBLICATIONS	II
III.	TABLE OF CONTENTS	III
IV.	ACKNOWLEDGEMENTS	VI
V.	STUDENT DECLARATION.....	VII
VI.	SIGNED AUTHOR DECLARATION – MINERAL LIBRARY PUBLICATION	VIII
VII.	SIGNED AUTHOR DECLARATION – ICELANDIC TEPHRA PUBLICATION	IX
VIII.	LIST OF ABBREVIATIONS	XI
IX.	LIST OF FIGURES.....	XIII
X.	LIST OF TABLES.....	XIX
1	GENERAL INTRODUCTION.....	2
1.1	RATIONALE FOR THIS THESIS AND BACKGROUND	2
1.2	BASALTS, PRIMARY AND SECONDARY MINERALOGIES, AND ANALYTICAL METHODS	3
1.3	BASALTS AND SECONDARY MINERAL DISTRIBUTION ON MARS	6
1.4	OVERVIEW OF ANALYTICAL TECHNIQUES EMPLOYED IN THE STUDY OF BASALTS AND MINERALS	11
1.4.1	<i>Vibrational Spectroscopy</i>	12
1.5	LIST OF METHODS USED IN THIS THESIS	14
1.5.1	<i>Sample preparation</i>	14
1.5.2	<i>Raman Spectroscopy</i>	14
1.5.3	<i>Fourier Transform Infrared Spectroscopy</i>	15
1.5.4	<i>Scanning Electron Microscopy</i>	15
1.5.5	<i>Electron Probe Microanalysis</i>	16
2	RAMAN CHARACTERISATION OF THE PRODUCTS OF ALTERATION OF VOLCANIC ROCK MINERALS.....	17
2.1	INTRODUCTION	18
2.2	PUBLISHED PAPER.....	20
2.2.1	<i>Summary</i>	20
2.2.2	<i>Introduction</i>	21
2.2.3	<i>Materials and Methods</i>	24
2.2.4	<i>Results</i>	27
2.2.5	<i>Interpretation: opportunities and challenges</i>	31
2.2.6	<i>Conclusions</i>	33

3	ANALYSIS OF ICELANDIC TEPHRA MINERALS.....	34
3.1	INTRODUCTION	35
3.2	PUBLISHED PAPER.....	37
3.2.1	<i>Abstract</i>	37
3.2.2	<i>Introduction</i>	38
3.2.3	<i>Geological Setting</i>	41
3.2.3.1	Iceland	41
3.2.3.2	Katla volcanic system	42
3.2.4	<i>Methodology</i>	45
3.2.4.1	Sample description.....	45
3.2.4.2	XRD.....	46
3.2.4.3	Raman spectroscopy	48
3.2.4.4	FTIR Spectroscopy	49
3.2.5	<i>Results</i>	50
3.2.5.1	XRD.....	50
3.2.5.2	Raman Spectroscopy	51
3.2.5.3	FTIR Spectroscopy	55
3.2.6	<i>Discussion</i>	56
3.2.7	<i>Acknowledgements</i>	58
4	EPMA, SEM AND RAMAN ANALYSIS OF EUCRITIC METEORITES FROM AUSTRALIA	59
4.1	INTRODUCTION	60
4.2	METEORITE CLASSIFICATION	62
4.2.1	<i>Asteroid IV Vesta</i>	65
4.3	SAMPLES	68
4.3.1	<i>Binda</i>	68
4.3.2	<i>Camel Donga</i>	70
4.3.3	<i>Millbillillie</i>	71
4.4	METHODOLOGY	75
4.4.1	<i>Raman Spectroscopy</i>	75
4.4.2	<i>Scanning Electron Microscopy (SEM)</i>	76
4.4.3	<i>Electron Probe Microanalysis (EPMA)</i>	76
4.5	RESULTS	77
4.5.1	<i>Binda</i>	77
4.5.2	<i>Camel Donga</i>	83
4.5.3	<i>Millbillillie</i>	90
4.6	DISCUSSION	96
4.6.1	<i>A discussion of analytical procedures and result comparisons</i>	99
5	SUMMARY AND FUTURE WORK.....	100

5.1	SUMMARY	101
5.2	FUTURE APPLICATIONS AND RESEARCH	102
6	REFERENCES	103
7	APPENDIX	136
7.1	MINERAL LIBRARY	136
7.1.1	<i>Sample Images</i>	136
7.1.2	<i>Raman Analyses</i>	136
7.1.3	<i>FTIR Spectra</i>	136
7.1.4	<i>Mineral Library Summary</i>	136
7.1.5	<i>LA-ICPMS</i>	136
7.2	ICELANDIC TEPHRA	136
7.2.1	<i>Sample Images</i>	137
7.2.2	<i>Raman Analyses</i>	137
7.2.3	<i>FTIR</i>	137
7.3	METEORITES	137
7.3.1	<i>Sample Images</i>	137
7.3.2	<i>Raman Analyses</i>	137
7.3.3	<i>Scanning Electron Microscopy</i>	139
7.3.3.1	SEM Images	140
7.3.3.2	SEM Tables	150
7.3.4	<i>Electron Microprobe</i>	156

IV. Acknowledgements

I would like to first and foremost thank all of my supervisors and advisers who have guided, assisted, and encouraged me over the last few years – Graziella Caprarelli, Barbara Stuart, Linda Xiao, Kelsie Dadd, Ross Pogson and Ronald Shimmon. Their dedication and belief in my abilities has been an inspiration, especially through the most difficult times. They have gone above and beyond to provide the support I have needed to finish.

The Australian Museum and Ross Pogson (Collection Manager: Mineralogy) have been instrumental in providing relevant samples for analysis imparting a wealth of knowledge.

I would also like to thank my friends and family for their patience and support, without which I would not have been able to complete this work – Kristina Bathgate, Simon Bathgate, Rebecca Gray, Ellen Curtis, Alicia Cook, Daniela Williams, Seth Williams, Alex Jarman, Rachel Gray, Frances Gray, Tony Gray, Nicola and Hugh Harricks, Bill White and Irene White.

I greatly appreciate the inspiration that my fellow colleagues and academics: Andrea Leigh, Finbarr Horgan, Helen Maynard-Casely, Fraser Torpy, William Gladstone and Brian Reedy have shared. Their vast collective knowledge has been essential in my completion of this thesis.

A huge thankyou also needs to go to everyone at EcoLogical Australia for their support in helping me finish my studies. A huge shout out to Nathan Kearnes, Robert Mezzatesta, Sophie Powrie and Beth Medway, without their continued support I would not have been able to finish this work.

V. Student Declaration

I, Emily Bathgate declare that this thesis, is submitted in fulfilment of the requirements for the award of Master of Science (Research) at the University of Technology Sydney.

This thesis is wholly my own work unless otherwise referenced or acknowledged. In addition, I certify that all information sources and literature used are indicated in the thesis. The multiple authorship of the published papers included in the thesis (highlighted in Chapters 2 and 3, with full text appended as indicated in the thesis) reflects the composition of the supervisory team, and additionally includes co-authors who provided samples and/or data by additional techniques, which were important for a complete interpretation of the work. These contributions have all been reported in the thesis as needed.

This document has not been submitted for qualifications at any other academic institution.

This research was supported by the Australian Government Research Training Program Scholarship.

Figures

All figures in this thesis are original and were made by Emily Bathgate unless otherwise indicated. No parts of these figures may be used for other purposes without the express permission of the author. For permission to reproduce any part of these figures please contact the Faculty of Science at the University of Technology Sydney.

Word Count

The word count of this thesis is 25,209

Signature: Production Note:
Signature removed prior to publication.

Date: 10/04/2019

VI. Signed Author Declaration – Mineral Library Publication

Raman characterisation of the products of alteration of volcanic rock minerals: preliminary results and implications for Martian studies

Emily Bathgate^{1-2*}, Graziella Caprarelli¹, Linda Xiao², Ron Shimmon², Ross Pogson³

1. School of the Environment, Faculty of Science, University of Technology, Sydney. PO Box 123, Broadway, NSW 2007, Australia. 2. School of Chemistry and Forensic Science, University of Technology, Sydney, PO Box 123, Broadway, NSW 2007, Australia. 3. Research and Collections, Geosciences and Archaeology, Australian Museum, 6 College St, Sydney, NSW 2010

**Corresponding Author: Emily.Bathgate@student.uts.edu.au*

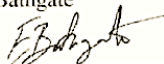
Emily Bathgate performed all laboratory work, data archiving and maintenance, data analysis, data interpretation, and wrote the manuscript.

Graziella Caprarelli (Principal Supervisor) provided the rationale for the project, collaborated on data analysis and interpretation, and edited the manuscript.

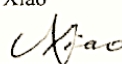
Linda Xiao and Ron Shimmon provided training in laboratory techniques and technical assistance during the laboratory work.

Ross Pogson supplied the samples and contributed to the analysis of the data.

Emily Bathgate



Linda Xiao



Graziella Caprarelli



Ron Shimmon



Ross Pogson



VII. Signed Author Declaration – Icelandic Tephra Publication

Raman, FTIR and XRD study of Icelandic tephra minerals: Implications for Mars

Emily J. Bathgate¹, Helen E. Maynard-Casely², Graziella Caprarelli³, Linda Xiao¹, Barbara Stuart¹, Kate T. Smith⁴ and Ross Pogson⁵

¹ School of Chemistry and Forensic Science, University of Technology Sydney, PO Box 123, Broadway, NSW 2007, Australia. ² Bragg Institute, Australian Nuclear Science and Technology Organisation, Locked Bag 2001, Kirrawee DC, New South Wales, 2232, Australia. ³ Division of IT, Engineering and the Environment (DITEE), University of South Australia, City East Campus, B13-49, Frome Road, Adelaide SA 5001, Australia. ⁴ Geography, College of Life and Environmental Science, University of Exeter, Penryn Campus, Treliwer Road, Penryn, Cornwall, TR10 9FE, UK ⁵ Research and Collections, Geosciences and Archaeology, Australian Museum, 6 College St, Sydney, NSW 2010

Emily Bathgate performed all the laboratory work for the Raman spectroscopy and FT-IR sections, analysis and interpretation of Raman spectroscopy and FT-IR data, and wrote all sections of the manuscript, except the section on XRD data.

Helen E. Maynard-Casely provided the rationale for the project, performed the XRD laboratory work, analysis and writing for that section as well as editorial input for the manuscript.

Graziella Caprarelli assisted with Raman spectroscopy and the interpretation of the Raman data, and edited the manuscript.

Linda Xiao and Barbara Stuart provided training in Raman techniques and guidance during the data acquisition.

Kate T. Smith provided the samples, insight to data analysis and Figure 1.

Ross Pogson contributed to the data analysis.

Emily Bathgate

Helen E. Maynard-Casely

Graziella Caprarelli

Linda Xiao

Barbara Stuart

Kate T. Smith

Production Note:
Signatures removed
prior to publication.

Production Note:
Ross Pogson Signature removed
prior to publication.

VIII. List of Abbreviations

CCD – Charge-Coupled Device

CRISM – Compact Reconnaissance Imaging Spectrometer

EBSD – Electron Back-Scattered Diffraction

EPMA – Electron Probe Microanalysis

ESA – European Space Agency

EVZ – Eastern Volcanic Zone

FTIR – Fourier Transform - Infrared

HED – Howardite-Eucrite-Diogenite

INAA – Induction Neutron Activation Analysis

ISAR – International Space Analogue Rockstore

ISM – Infrared Spectrometer

LOD – Limit of Detection

MGS – Mars Global Surveyor

MORB – Mid-Ocean Ridge Basalts

MRO – Mars Reconnaissance Orbiter

NAIP – North Atlantic Igneous Province

NASA – National Aeronautics and Space Administration

NVZ – Northern Volcanic Zone

OIB – Ocean Island Basalts

REE – Rare Earth Elements

RLS – Raman Laser Spectrometer

SEM – Scanning Electron Microscopy

SNC – Shergotty-Nakhla-Chassigny

TES – Thermal Emission Spectroscopy

WVZ – Western Volcanic Zone

XRD – X-Ray Diffraction

XRF – X-Ray Fluorescence

IX. List of Figures

- Figure 1 - Petrogenetic grid for metamorphism of basaltic rocks assuming an intermediate oxidation state and an aqueous fluid (Figure after Ernst 1993). Numbers indicating P-T ranges of facies as in Table 1. The facies are named after the most characteristic mineral of the metamorphic assemblage (zeolite, prehnite-pumpellyite), or by rock type (e.g., amphibolite). Dashed lines represent the gradients of pressure and temperature of typical tectonic settings. 5
- Figure 2 - Distribution of Surface Type 1 and Surface Type 2: red indicates higher concentrations and blue indicates lower concentrations of the surface types (Bandfield et al. 2000)..... 7
- Figure 3 - Clay mineral distribution and diversity grouped according to their geological settings (Ehlmann et al. 2011). Open diamonds represent CRISM images with no clay detection and filled diamonds represent detections of clay minerals. 8
- Figure 4 - Comparison of chronologies of Mars developed using crater chronology and mineral assemblages..... 9
- Figure 5 - Compositional ternary diagram depicting chemical and mineral changes caused by aqueous alteration of basalts (Ehlmann et al. 2011). Open squares represent the stoichiometry of pure clay mineral phases. The position of terrestrial basalts is shown, and the arrows indicate path of alteration in conditions of high water/rock ratios (dark purple colour area) or low water/rock ratios (green, red and yellow areas). Open triangles represent chemical compositions of martian clays. These compositions are characteristic of low water/rock ratios. 10
- Figure 6 - Microscopic images of common primary and secondary basaltic minerals: (a) olivine; (b) labradorite; (c) analcime; (d) muscovite; (e) natrolite (crystal width: 0.254 mm); (f) nontronite. All microphotographs were taken with a light microscope at 35x magnification. Scale bars: 2 mm..... 25
- Figure 7 - Simplified schematic diagram of the Raman spectrometer used in this work. The monochromatic light source is focused onto the sample through the microscope objective. The elastically scattered light is removed by the notch

filter. The weaker Raman scattered light is focused onto a diffraction grating and then processed by the CCD. The signals are processed by the software and a binary plot of Raman shift and signal intensity is obtained as analysis output. 26

Figure 8- Results: (a) Orientation effects for olivine in the 120-1800 cm^{-1} spectral range where spectra 1-5 are the five readings taken at different orientations of the sample, major spectral changes indicated by arrows, (b) Orientation effects for muscovite in the 120-1800 cm^{-1} spectral range where spectra 1-5 are the five readings taken at different orientations of the sample muscovite: no major spectral changes with orientation. The muscovite crystal was oriented perpendicular to the excitation source, which corresponds to a symmetric direction of the minerals in which all directions are equivalent relative to the beam, (c) Higher range spectra of selected hydrated minerals: serpentine, chlorite, nontronite, prehnite and natrolite. All of these secondary minerals have structural water and show a distinctive peak in this range: serpentine, 3685 and 3698 cm^{-1} ; chlorite, 3681 cm^{-1} ; nontronite, 3579 cm^{-1} ; prehnite, 3482 cm^{-1} ; natrolite, 3325 and 3526 cm^{-1} , (d) Clays: Raman spectra of saponite (red) and kaolinite (blue). The sample of saponite has no distinguishing peaks. The sample of kaolinite has one distinguishing peak at 142 cm^{-1} 28

Figure 9 - Map of Iceland showing the NVZ, EVZ and the WVZ. The approximate locations of the Katla volcano and the Eldgjá fissure in the EVZ are indicated by the triangles. (Base map data from National Land Survey of Iceland, approximate extents of volcanic zones after Sigmarsson & Steinthórsson 2007). 43

Figure 10 - Flow chart illustrating which methods were used on the different sample aliquots. The micronized samples were used for XRD, Raman spectroscopy and FTIR. The unprocessed samples were used for Raman spot sampling. The micronized samples were used for Raman mapping as a flat surface could be achieved due to small grain size. This allowed for the collection of 350-400 spectra per sample for analysis. 49

Figure 11 - Rietveld refinement mineral fitting in the TOPAS suite (Coelho 2008) to samples 2 (A) and 3 (B). The crystal structures used to determine these fits were obtained from the American Mineral Database (Downs & Hall-Wallace 2003). The observed patterns were collected at a wavelength of $\lambda = 0.9535 \text{ \AA}$, in

transmission geometry. Below the observed pattern are the fitted contributions from the amorphous component of the pattern (fitted with three pseudo-voigt peaks), labradorite, augite and magnetite (both samples) and ilmenite and fluoroapatite (sample 3). The contribution to the fit of the fluorite standard to sample 2 is omitted for clarity, but the fluorite peaks are indicated with asterisks.	50
Figure 12 - Raman spectroscopy: spectra of selected minerals from Katla volcano. (A) Anatase obtained from sample 1, collected by 785 nm laser source. (B) Examples of pyroxene and hematite, collected by 633 nm laser source from sample 2. (C) Magnetite, pyroxene and olivine obtained from sample 3 (633 nm). (D) Spectrum of ulvospinel from sample 4 (633 nm). (E) Spectra obtained from sample 5 of plagioclase and pyroxene (633 nm). (F) Obtained from sample 6 of plagioclase and ulvospinel (633 nm).	53
Figure 13 - Selected Raman results from the Eldgjá fissure. Pyroxene, olivine, hematite and magnetite from sample 12.	55
Figure 14 - FTIR Spectrum of Sample 1 showing the peaks common to all samples (at $\sim 3400\text{ cm}^{-1}$, $\sim 1635\text{ cm}^{-1}$ and the large broad peak from $1100\text{-}900\text{ cm}^{-1}$).	56
Figure 15 - Ages of eucrites. Summary of key dates obtained from eucritic meteorites using different dating systems (Bogard & Garrison 2003; Boyet, Carlson & Horan 2010; Manhès, Allegre & Provost 1984; Misawa, Yamaguchi & Kaiden 2005). Sm/Nd ages of Binda, U-Pb and Pb isotope ages of various eucrites, U-Th-Pb age of JUVINAS (a representative eucrite) and Ar isotope ages of various eucrites.	61
Figure 16 - Simplified Meteoritic Classification (modified from Weisberg, McCoy & Krot (2006)).	62
Figure 17 - Images of Asteroid IV Vesta taken from the Dawn Spacecraft's framing camera. These images illustrate the varied surface of the asteroid with striations along the surface around the equator, numerous impact craters and mountainous regions. Image resolution: $\sim 500\text{ m/pixel}$. Image credit: NASA/JPL-Caltech/UCLA/MPS/DLR/IDA.	66
Figure 18 - Proposed model for the formation of Asteroid IV Vesta and the origin of eucrites (Figure from Mandler & Elkins-Tanton 2013).	68
Figure 19 - Map of locations where meteorites were found and collected	69

Figure 20 - Photographs of the whole Binda meteorite specimen from the Australian Museum, note the fusion crust with observable ablation flow.....	77
Figure 21 - Plain polar image (left) and crossed polar image (right) of Binda at 50x showing large pyroxene crystal and surrounding matrix. Field of view: 4.75 x 3.05 mm.	78
Figure 22 - SEM image of Binda meteorite, showing baddeleyite (bright), surrounded by pyroxene. The relevant EDS spectra are labelled 126-170, and are included in Appendix 7.3.4.....	79
Figure 23 - Raman result for magnetite from Binda meteorite Area 4 matched to RRUFF tm Project database R061111.	80
Figure 24 - Raman baddeleyite (a zircon mineral) from Binda meteorite Area 4. Baddeleyite spectrum was compared to the RRUFF tm Project database spectrum with main diagnostic peaks at 178, 189, 223, 307, 381, 476, 501, 539, 558, 617 and 638 cm ⁻¹ matching the RRUFF tm Project database spectrum R060016. All peaks in the spectrum match the library spectrum for baddeleyite except the two highlighted. We obtained a strong peak at 334 cm ⁻¹ whereas the library spectrum contained two weaker peaks in this area. We also obtained a strong peak at 688 cm ⁻¹ whereas the library spectrum contained a very weak peak ~700 cm ⁻¹ . These differences may be due to slight compositional differences or other compounding minerals.	80
Figure 25 - Raman map of Binda meteorite Area 4 illustrating baddeyleite, magnetite and two different structures of pyroxene.	81
Figure 26 - Raman result for pyroxene (1) (matched to RRUFF tm Project database enstatite R040093 or diopside R060861) visible in Raman map from Binda meteorite.....	82
Figure 27 - Raman result for pyroxene (2) (Matched to RRUFF tm Project database R040097) visible in Raman map from Binda meteorite.	82
Figure 28 - Photograph of whole Camel Donga meteorite specimen from the Australian Museum.	83
Figure 29 - Plain polar image (left) and crossed polar image (right) of Camel Donga at 100x illustrating breccia like material. Field of view: 2.33 x 1.53 mm.	84
Figure 30 - Plain polar image (left) and crossed polar image (right) of Camel Donga at 100x illustrating high metal oxide content. Field of view: 2.33 x 1.53 mm. .	85

Figure 31 - SEM image of Camel Donga from Area 1 illustrating a large metal and oxide mass (bright white). The relevant EDS spectra are labelled 159-199 and are included in Appendix 7.3.3.	85
Figure 32 - Raman of labradorite or anorthite from Camel Donga Area 2 matching RRUFF tm Project database labradorite (R060221) and anorthite (R040059) with main diagnostic peak at 505 cm ⁻¹	86
Figure 33 - Raman result for pyroxene diopside or ferrosilite from Camel Donga Area 1. Matched to RRUFF tm Project database diopside (R060861).	86
Figure 34 - Raman result for pyroxene diopside from Camel Donga Area 1, matched to RRUFF tm Project database diopside (R060861).	87
Figure 35 - Raman result for iron oxides. Mixed spectrum of magnetite (main peak at 678 cm ⁻¹) and hematite (main peaks at 219 cm ⁻¹ and 278 cm ⁻¹) from Camel Donga Area 1. Magnetite matched to RRUFF tm Project database (R061111). .	87
Figure 36 - Raman result of iron oxide mineral hematite (main peaks at 225 cm ⁻¹ and 293 cm ⁻¹) from Camel Donga Area 1. Hematite matched to RRUFF tm Project database (R050300).....	88
Figure 37 - Raman from Camel Donga Area 1 showing two products of preparation, diamond (1329 nm) and quartz (464 nm). Matched to RRUFF tm Project database diamond (R050206) and quartz (X080016).	88
Figure 38 - Whole Millbillillie specimen from the Australian Museum.	90
Figure 39 - Plain polar image (left) and crossed polar image (right) of Millbillillie at 50x, illustrating pyroxenes, opaque material (oxides) and fractured plagioclase illustrative of impacts. Field of view: 4.75 x 3.05 mm.	91
Figure 40 - Raman result for pyroxene from Millbillillie meteorite Area 1 matching RRUFF tm Project database ferrosilite (R070386)	92
Figure 41 - Raman result of second pyroxene structure in Millbillillie meteorite Area 1. Matching spectrum of ferrosilite from RRUFF tm Project database R070387.	93
Figure 42 - SEM image from Millbillillie Area 1 illustrating large pyroxene crystal with surrounding plagioclase and oxides. The relevant EDS spectra are labelled 171-250, and are included in Appendix 7.3.3.	93
Figure 43 - Mapping results from Millbillillie meteorite. Intensity at point map, bright red illustrates areas where the peak at 464 cm ⁻¹ occurs and darker areas show where it does not occur. The peak at 464 cm ⁻¹ is the diagnostic peak of	

quartz. The bright red areas show where the gaps in the minerals are located.

The plain light image behind shows context of the location of the oxide..... 94

Figure 44 - Mapping results from Millbillillie meteorite. Intensity at point map, bright red illustrates areas where the peak at 280 cm^{-1} occurs and darker areas show where it does not occur. The left hand side of the opaque material is mostly hematite. 94

Figure 45 - Mapping results from Millbillillie meteorite. Intensity at point map, bright red illustrates areas where the peak at 677 cm^{-1} occurs and darker areas show where it does not occur. The right hand side of the mapped area is mostly ilmenite with the transition area spectra exhibiting peaks from both end-member oxides. 95

Figure 46 - Pyroxene quadrilateral. Data points corresponding to the pyroxene quadrilateral components corrected for Na and Al contents are plotted, together with Lindsley and Anderson's (1983) 1 bar isotherms (dashed lines)..... 97

X. List of Tables

Table 1 – The ten major metamorphic facies of basalt and their minerals (modified after Duff 1993) numbers indicate the P-T fields of each facies represented in the petrogenetic grid of Figure 1	6
Table 2 - List of reference minerals obtained for the calibration database. Entries in italics indicate hydrated minerals.....	24
Table 3 - Provenance and composition of tephra examined	46
Table 4 - Summary of Raman and XRD results from samples 1-6 and 12. For XRD results GOOF indicates goodness of fit and wRp indicates the weighted residual for the fit of all components to the pattern. (*early indication of the presence of these minerals indicated by Raman, to be confirmed by XRD).....	54
Table 5 - Summary of FTIR results for samples 1-6 and 12. (Strength of peaks in spectrum: s = strong, m = medium, w = weak, and b = broad)	56
Table 6 - Representative analyses of plagioclases	78
Table 7 - Composition of Binda pyroxenes	79
Table 8 - Composition of Camel Donga pyroxenes.....	84
Table 9 - Composition of Millbillillie pyroxenes	92